



NRC Publications Archive Archives des publications du CNRC

Snow drifts on flat roofs : wind tunnel tests and field measurements da Matha Sant'Anna, F.; Taylor, D. A.

This publication could be one of several versions: author's original, accepted manuscript or the publisher's version. /
La version de cette publication peut être l'une des suivantes : la version prépublication de l'auteur, la version
acceptée du manuscrit ou la version de l'éditeur.

Publisher's version / Version de l'éditeur:

Journal of Wind Engineering and Industrial Aerodynamics, 34, 3, pp. 223-250,
1990-08

NRC Publications Record / Notice d'Archives des publications de CNRC:

<https://nrc-publications.canada.ca/eng/view/object/?id=ed70dc40-7dea-4315-a27c-09fbbc337545>
<https://publications-cnrc.canada.ca/fra/voir/objet/?id=ed70dc40-7dea-4315-a27c-09fbbc337545>

Access and use of this website and the material on it are subject to the Terms and Conditions set forth at

<https://nrc-publications.canada.ca/eng/copyright>

READ THESE TERMS AND CONDITIONS CAREFULLY BEFORE USING THIS WEBSITE.

L'accès à ce site Web et l'utilisation de son contenu sont assujettis aux conditions présentées dans le site

<https://publications-cnrc.canada.ca/fra/droits>

LISEZ CES CONDITIONS ATTENTIVEMENT AVANT D'UTILISER CE SITE WEB.

Questions? Contact the NRC Publications Archive team at
PublicationsArchive-ArchivesPublications@nrc-cnrc.gc.ca. If you wish to email the authors directly, please see the
first page of the publication for their contact information.

Vous avez des questions? Nous pouvons vous aider. Pour communiquer directement avec un auteur, consultez la
première page de la revue dans laquelle son article a été publié afin de trouver ses coordonnées. Si vous n'arrivez
pas à les repérer, communiquez avec nous à PublicationsArchive-ArchivesPublications@nrc-cnrc.gc.ca.



Ser
TH1
N21d
no. 1689
c. 2
BLDG

**National Research
Council Canada**

**Conseil national
de recherches Canada**

**Institute for
Research in
Construction**

**Institut de
recherche en
construction**

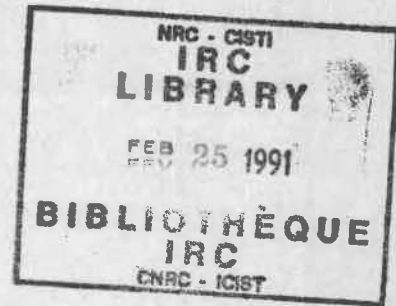
Snow Drifts on Flat Roofs: Wind Tunnel Tests and Field Measurements

by F. Da Matha Santanna and D.A. Taylor

ANALYZED

Reprinted from
Journal of Wind Engineering and Industrial Aerodynamics,
34 (1990) 223-250
Elsevier Science Publishers B.V., Amsterdam
(IRC Paper No. 1689)

NRCC 32359



CISTI / ICIST



3 1809 00210 7438

Résumé

On a mis au point des règles de mise à échelle pour concevoir des expériences et choisir des particules en vue de la modélisation, dans une soufflerie aérodynamique à couche limite, des amoncellements de neige sur les bâtiments. Plusieurs maquettes de bâtiments à toit plat à deux niveaux ont été étudiées dans la soufflerie. Le rapport longueur-hauteur des bâtiments variait entre 1,0 et 10,0, et la longueur des niveaux inférieurs variait entre 1,3 et 5 fois leur hauteur aux niveaux supérieurs. Pour évaluer les hauteurs de simili-neige après chaque essai, on a utilisé un appareil de mesure tridimensionnelle à course transversale muni d'un indicateur de hauteur. Deux bâtiments à toit plat situés à Ottawa (Canada) ont été choisis aux fins de comparaison des mesures en soufflerie et de celles en vraie grandeur. L'écart entre les résultats des essais en vraie grandeur et ceux des essais sur maquettes tient en partie à des conditions de réalisation différentes : les changements de direction du vent n'ont pu être pris en compte parce que les maquettes étaient trop longues pour effectuer une rotation complète dans la soufflerie. Les similarités entre les hauteurs de neige à l'échelle réduite et à l'échelle réelle sont assez nombreuses pour justifier des recherches plus poussées dans une soufflerie plus grande.

SNOW DRIFTS ON FLAT ROOFS: WIND TUNNEL TESTS AND FIELD MEASUREMENTS

F. DA MATHA SANT'ANNA* and D.A. TAYLOR

*Structures Section, Institute for Research in Construction, National Research Council,
Ottawa, K1A 0R6 (Canada)*

(Received August 23, 1985; accepted in revised form April 4, 1990)

Summary

Scaling rules are developed for the design of experiments and choice of appropriate particles to model snow drifting on buildings in a boundary-layer wind tunnel. Several model buildings with two-level flat roofs were studied in the tunnel. The length-to-height ratios of the buildings varied from 1.0 to 10.0 and the lengths of lower roofs varied from 1.3 to 5 times the heights to the upper levels. A three-dimensional traversing mechanism holding a depth-marker was used for collecting "snow" depths after each test. Two flat-roofed buildings in Ottawa, Canada, were selected for comparison of wind tunnel with full-scale measurements. The discrepancy between results of full-scale and model-scale testing is due in part to dissimilar running conditions: the changes in wind directions could not be followed because the model buildings were too long to be rotated fully in the wind tunnel. There are enough similarities between model and full-scale snow depths to indicate that further investigation with a larger wind tunnel would be worthwhile.

1. Introduction

In 1982 research on modelling the formation of snow drifts on roofs was started at the Institute for Research in Construction, National Research Council of Canada. The aim was to simulate depths of snow drifts on roofs using models in a wind tunnel.

(1) Scaling relations were developed for simulating snow drifting on buildings in a thick boundary-layer wind tunnel. These allowed the selection of particles to model the snow.

(2) A water tunnel was used for visualizing flow behaviour around two-level flat roofs as an aid to understanding the drifting process.

(3) Wind tunnel tests were done and the results compared with field measurements of snow drifts on two two-level flat roofs obtained during a 15 year survey.

*Present address: 1785-F Lamoureux Drive, Orleans, Ont., K1E 2H3, Canada.

2. Particle and time scaling

2.1. Introduction

For modelling of snow transported by saltation, particles are scaled to achieve geometric, kinematic, and dynamic similarity. Scaling requirements can be derived from a particle trajectory (Fig. 1) to give the following relation between velocities and forces [1]

$$\ddot{x} + \frac{K_0}{M} \dot{x} = \frac{K_0}{M} K_1 y \quad (1)$$

and

$$\ddot{y} + \frac{K_0}{M} \dot{y} + g = 0 \quad (2)$$

In eqn. (1), x is the horizontal distance in the direction of particle movement and y is the distance above the floor of the tunnel; the drag force D is equal to $K_0 u_r$, where u_r is the velocity of the particle relative to the fluid and K_0 is a constant of proportionality related to "d", the particle diameter. The vertical velocity component of the fluid is assumed to be zero; therefore the second term in eqn. (2) will be zero. Further, the velocity profile is assumed to be linear within the thick, turbulent, boundary-layer where y is less than the roughness length, z_0 . Thus $V = K_1 y$ where V is the local fluid velocity at the particle; g is the gravitational acceleration.

In addition, the following is assumed.

(1) The thickness δ of the boundary layer is not a relevant parameter because

$$h_0 \ll H \ll \delta \quad (3)$$

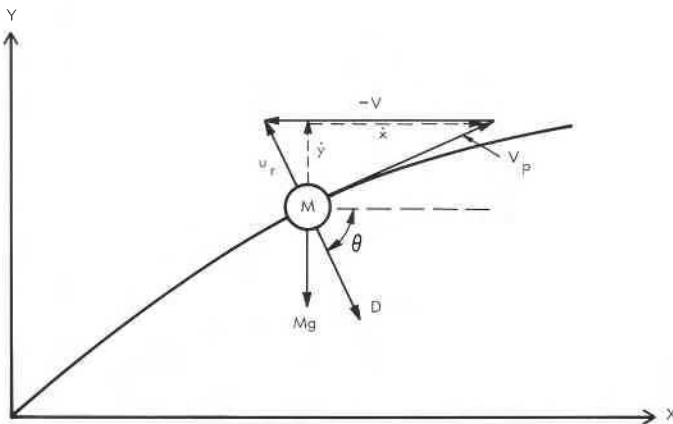


Fig. 1. Trajectory of a particle of mass M .

where h_0 is the height of the roughness elements in the upstream boundary layer and H is the height of the model building. Further, the model building is sharp edged causing a well defined separation bubble downstream.

(2) The model height H is the only length scale imposed on the flow.

(3) Flow is independent of viscosity if

$$\text{Re}_{y_H} \gg 1 \quad (4)$$

River silt and, in moving air, sand, dust and snow rise from the surface as "clouds" of particles [2-6]. The clouds are thrown up by surface eddies and may penetrate into the mean flow [7-9]. The authors observed such clouds over models of flat-roofed buildings in water tunnel experiments which they performed prior to using the wind tunnel (Figs. 2 and 3). Such experiments show approximate mean flow patterns over flat-roofed buildings due to flow separation.

From observations of flow over models in the water tunnel (Figs. 2(a), (b)) it appears that the separation bubble collapses periodically and that vortices from the collapsing bubble become a downstream-moving vortex system (location N in Fig. 2(b)). This vortex system moves the "cloud" of particles until

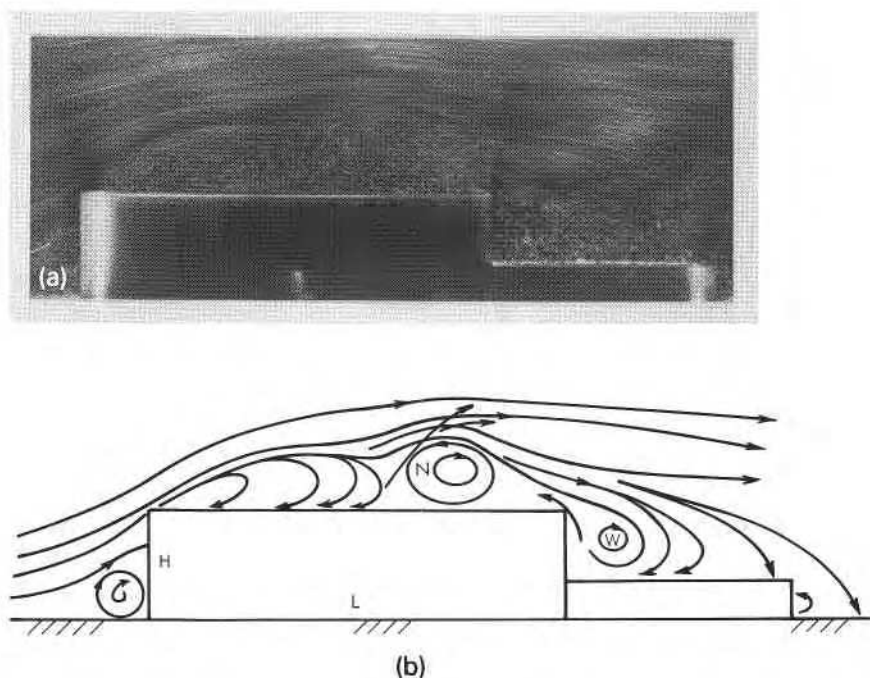


Fig. 2. Flow behaviour around a two-dimensional bluff body (building with two-level flat roof) in a water tunnel, showing collapsing and rolling bubble, $L/H=3.74$ and $\text{Re}_y=10^4$. (b) Sketch of mean flow patterns over long building, indicating fully developed bubble at leading edge. The formation region is shown rolling up as vortex system N.

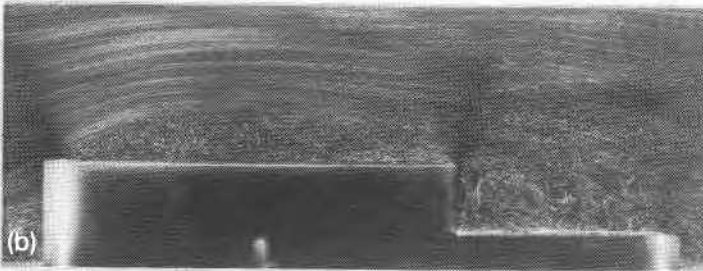
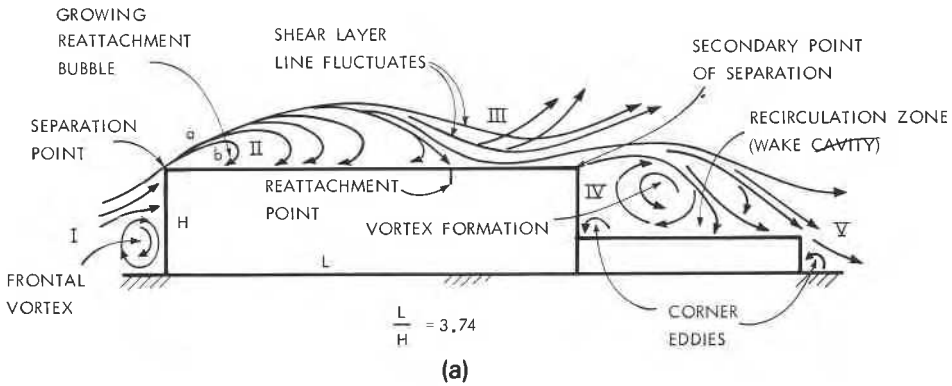


Fig. 3. (a) Approximate mean flow pattern over a building. Arrows show reverse flow and growing bubble. (b) Flow behaviour around a two-dimensional bluff body (building with a two-level flat roof) in a water tunnel, showing collapsing bubble exhausting into the near-wake. $L/H=3.74$ and $Re_y=10^4$.

the system breaks down and casts up particles into the near wake (W in Fig. 2(b)).

The dimension l of the "clouds" depends on the variation of the flow field near the model, the structure of the turbulence, and the velocity gradient in the shear layer. l is related to the turbulent convection process of the particles, l is chosen as a reference length of the micro scale of the motion of the solid particle [10]; thus the following non-dimensional parameters are obtained:

$$\bar{l} = \frac{l_m}{l} \quad \bar{U} = \frac{U_m}{U} \quad \bar{d} = \frac{d_m}{d} \quad \bar{\rho} = \frac{\rho_m}{\rho} \quad (5)$$

where l is as defined above, d is a characteristic dimension of a particle, and ρ is the characteristic density for a particle of mass M . The subscript m represents model scale conditions.

In addition, there is an approximate relationship assumed between l and

roughness length, z_0 which depends on the density of the roughness elements [8]:

$$l \propto z_0 \quad (6)$$

From eqns. 1 and 2 one can deduce the motion of a model scale particle (subscript m) of mass M ,

$$\ddot{x}_m + \frac{K_{0m}}{M_m} \dot{x}_m = \frac{K_{0m}}{M_m} K_{1m} y_m \quad (7)$$

and

$$\ddot{y}_m + \frac{K_{0m}}{M_m} \dot{y}_m + g = 0 \quad (8)$$

As explained in Appendix A, non-dimensional parameters introduced in eqns. 7 and 8 give:

$$\frac{\bar{U}^2}{\bar{l}} \ddot{x} + \frac{K_0}{M} \frac{\bar{U}}{\bar{\rho} \bar{d}^2} \dot{x} = \frac{K_0}{M} \frac{K \bar{l}}{\bar{\rho} \bar{d}^2} K_1 y \quad (9)$$

$$\frac{\bar{U}^2}{\bar{l}} \ddot{y} + \frac{K_0}{M} \frac{\bar{U}}{\bar{\rho} \bar{d}^2} \dot{y} + g = 0 \quad (10)$$

Strom et al. [1] obtained similar equations for trajectories of particles in the model tests in a wind tunnel.

2.2. Scaling requirements

Geometric similarity. The macro scale of the model building was assumed to be

$$\frac{\delta}{H} \gg 1 \quad (11)$$

From eqn. (11) one can obtain:

$$\left(\frac{\delta}{H} \right)_m = \left(\frac{\delta}{H} \right)_p \quad (12)$$

where m and p represent respectively model and prototype.

The micro scale of the motion of the solid particle

$$\frac{l_m}{l_p} \quad (13)$$

is chosen for particle geometric similarity [11] and thus

$$\frac{l_m}{l_p} = \frac{z_{0m}}{z_{0p}} \quad (14)$$

Dynamic similarity. From comparison of eqns. (9) and (10) and eqns. (1) and (2), the basic requirement for dynamic similarity,

$$\frac{\bar{U}^2}{\bar{l}} = 1 \quad (15)$$

may be obtained. In another form

$$\left(\frac{l_m}{l_p}\right)^2 = \frac{l_m}{l_p} = \left(\frac{z_{0m}}{z_{0p}}\right) \quad (16)$$

and finally from eqn. (5)

$$\frac{U_m}{U_p} = \left(\frac{z_{0m}}{z_{0p}}\right)^{1/2} \quad (17)$$

Density scaling requirements. The relation between physical characteristics of model and prototype can be obtained, as before, from eqns. (9) and (10) and eqns. (1) and (2). Thus

$$\frac{\bar{U}}{\bar{\rho}\bar{d}^2} = 1 \quad (18)$$

or

$$\frac{l_m}{l_p} = \frac{\rho_m}{\rho_p} \left(\frac{d_m}{d_p}\right)^2$$

and

$$\frac{\rho_m}{\rho_p} \left(\frac{d_m}{d_p}\right)^2 = \left(\frac{z_{0m}}{z_{0p}}\right)^{1/2} \quad (19)$$

where z_{0m} is obtained from the boundary-layer wind tunnel, and z_{0p} is an appropriate roughness length for local topography.

Kinematic similarity. The kinetic similarity is expressed in the form [6,12]

$$\left(\frac{U_{\text{TER}}}{u^*}\right)_m = \left(\frac{U_{\text{TER}}}{u^*}\right)_p \quad (20)$$

where U_{TER} is the mean terminal velocity of the particle and u^* the mean shear velocity.

It appears (Figs. 2 and 3) that the shear flow over the building causes an acceleration of the particles, while particles trapped in the reattachment bubble are decelerated. The mean velocity U_s at the separation point and the mean shear stress u_H^* at the model height are influential parameters. Thus the flowing relations apply for kinematic scaling:

$$\left(\frac{U_s}{u_H^*}\right)_m = \left(\frac{U_s}{u_H^*}\right)_p \quad \text{and} \quad \left(\frac{U_{\text{TER}}}{U_s}\right)_m = \left(\frac{U_{\text{TER}}}{U_s}\right)_p \quad (21)$$

These relations imply that the corresponding angles between the streamlines and paths (or waves) remain the same over model and full-scale buildings.

2.3. Time scaling

All stages of deposition in full and model scales are similar if the time scale is chosen properly. Newton's second law in non-dimensional form provides an adequate time scale for fully rough flow, with air as the medium in model and prototype (Appendix B):

$$\frac{t_m}{t_p} = \frac{\rho_m}{\rho_p} \frac{d_m}{d_p} \left(\frac{z_{0m}}{z_{0p}}\right)^{1/2} \quad (22)$$

The factor of d_m/d_p in eqn. (22) implies that drift profiles will be identical in model and field studies.

The micro scale of the solid particle (eqn. (14)), the physical relationship described in eqn. (19) and the time law (eqn. (22)) were all used as described in the following section, to choose the modelling particles and time scaling. Time scaling is required to predict final profile dimensions of drifts and provides information on drift evolution. Indeed the wind tunnel experiments in the following section are solely concerned with simulating drift geometry.

3. Wind tunnel measurements

3.1. Choice of modelling particles

Three types of particles – Ottawa sand, ground foam and sawdust – were examined for simulating snow drifting in the wind tunnel. Of these, sawdust passing a 0.297 mm mesh sieve and collected on a 0.250 mm sieve (average 0.274 mm characteristic dimension) was used in the model studies.

The ratio of sawdust to snow density ρ_m/ρ_p was taken to be 0.8 for the Ottawa area, (although snow density can vary enormously), and the ratio of characteristic dimension of the sawdust particles to snow particles was $d_m/d_p = 0.274/0.8$. Further, the characteristic length ratio, equal to the roughness ratio, is $l_m/l_p = z_{0m}/z_{0p} = 15/750 = 1/50$. Substitution in eqn. (19) gives:

$$\frac{\rho_m}{\rho_p} \left(\frac{d_m}{d_p}\right)^2 = 0.8 \left(\frac{0.274}{0.8}\right)^2 = 0.094$$

while

$$\left(\frac{z_{0m}}{z_{0p}}\right)^{1/2} = \left(\frac{1}{50}\right)^{1/2} = 0.141$$

Equation (19) is thus not fully satisfied.

Because of the considerable variability of real snow and the assumptions made in the development of the equations, the sawdust was nevertheless considered acceptable. Sawdust with a larger particle size should probably have been used. The time scaling was (eqn. (22)):

$$\frac{t_m}{t_p} = 0.8 \frac{0.274 \left(\frac{1}{50} \right)^{1/2}}{0.8} = \frac{1}{26}$$

Using the sawdust as described, a run time of 5 min in the wind tunnel is equivalent to just over 2 h of wind at full scale.

3.2. Experimental set-up

3.2.1. Environmental wind tunnel

The experiments reported here were performed in a 10 m long, 0.914 m \times 0.914 m open-circuit wind tunnel (Fig. 4). The width of the working section restricted testing of a full range of wind directions β for long models. The free-stream turbulence level was approximately 0.6% in the empty working section.

To establish mean velocity profiles and turbulence characteristics in good agreement with those of urban areas, surface roughness elements and a turbulence grid [13] were used. The power-law exponent α of the velocity profile obtained was 0.38; the roughness length z_0 was 15 mm, and the mean shear velocity u^* was 0.26 m s⁻¹. Variation of the longitudinal turbulence intensity based on the local mean velocity is illustrated in Fig. 5. The thickness of the boundary layer was 430 mm.

3.2.2. Traversing mechanism

A traversing mechanism capable of moving in three directions was mounted inside the low-speed test section after each experiment (see Fig. 6). All three

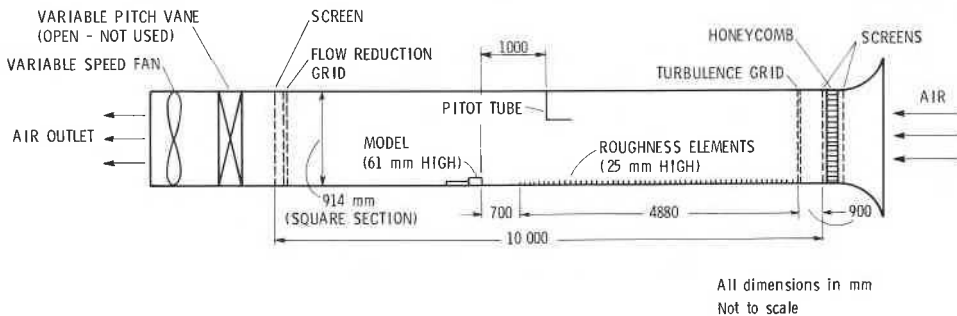


Fig. 4. Side view of the wind tunnel.

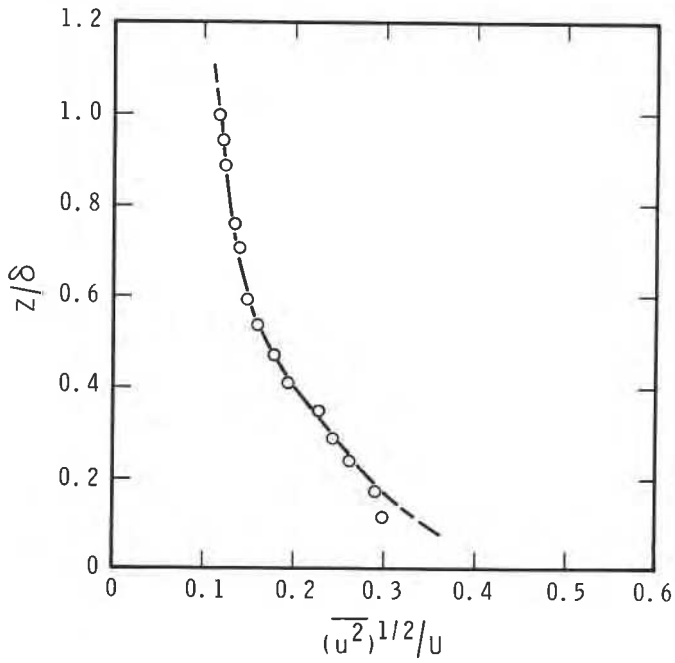


Fig. 5. Longitudinal component of turbulence intensity distribution at the model location.

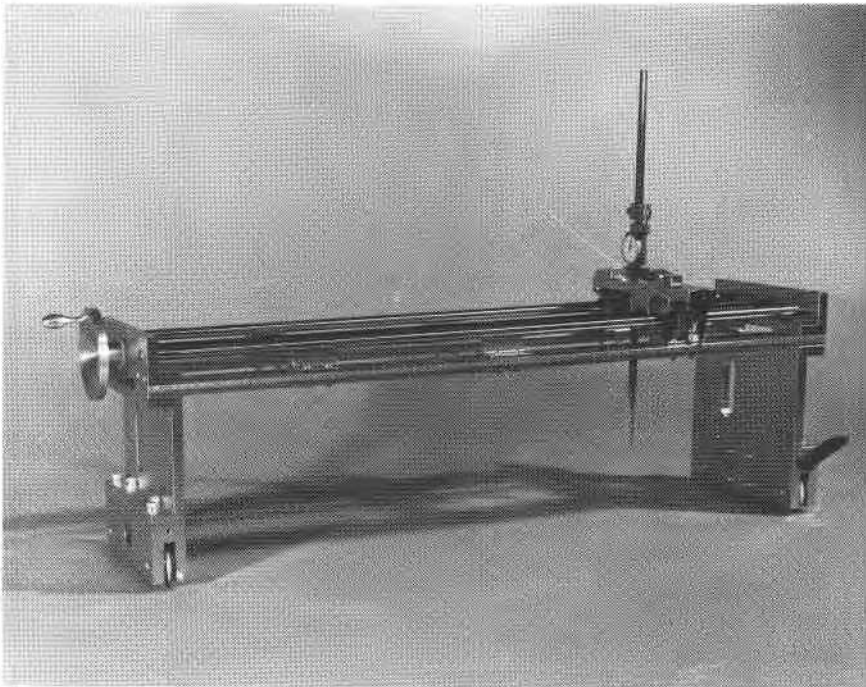


Fig. 6. Traversing mechanism with depth marker.

directions of motion are controlled manually to obtain depths of sawdust to within 0.05 mm at predetermined locations on the roofs after each test.

3.3. Testing procedure

Definition of some terms is required. "First fall" applies to snowfall accompanied by winds of about 0.60 m s^{-1} at the model height (or 4.25 m s^{-1} in full scale). "First drifting" applies to wind at 2.4 m s^{-1} (17 m s^{-1} full scale) without snowfall. Snowstorm effects are therefore identified by "first drifting, first fall" and "second drifting, first fall" etc. The ratio between model and full scale velocities are obtained from eqns. (16) and (17). Thus

$$\frac{U_m}{U_p} = \left(\frac{z_{0m}}{z_{0p}} \right)^{1/2} = (0.02)^{1/2} = \frac{1}{7.07}$$

In earlier experiments, particles were distributed to a uniform depth on the upper roof before the wind tunnel was turned on. This effectively increased the height of the building. Moreover the particles "smoothed" the leading edge and modified the characteristics of the reattachment bubble. As a result, this approach was abandoned and a two-step approach to testing was adopted. During the first step the particles were fed slowly through a slot in the roof of the tunnel 0.65 m upstream of the model while a light wind was blowing. This continued for 15 min, equivalent to a snowstorm of about 6.5 h. The free stream dynamic pressure at a height of 0.650 m above the tunnel floor and 1.0 m upstream of the model location was maintained at a constant value indicating a velocity of 0.91 m s^{-1} . The corresponding velocity at the model height measured by a hot wire anemometer was 0.60 m s^{-1} , equivalent to 4.25 m s^{-1} in full scale. During the second step a stronger wind of 2.4 m s^{-1} at the model height blew for about 5 min, simulating a windstorm of approximately 2 h. It redistributed the particles from the upper (windward) to the lower (leeward) roof in drifts like those formed in a real storm [6,7,14].

3.4. Wind tunnel results

The results of the experiments using sawdust as described in section 3.1 are presented in Figs. 7-13. $h_s/\Delta H$ and $l_s/\Delta H$ are plotted against the aspect ratio L/H (Fig. 11) and building separation ratio S/H (Fig. 13). The drift on the lower of a two-level flat roof is seen to vary with the wind direction and the aspect ratio L/H of the upper building (Figs. 9 and 10), and with the difference in elevation ΔH between the upper and lower roofs. H and L are the height and length of the building, and h_s and l_s are the height and length of the drift on the lower roof (Figs. 7-13).

3.4.1. Estimate of the drift height h_s

Case I: $\Delta H/H = 1/2$.

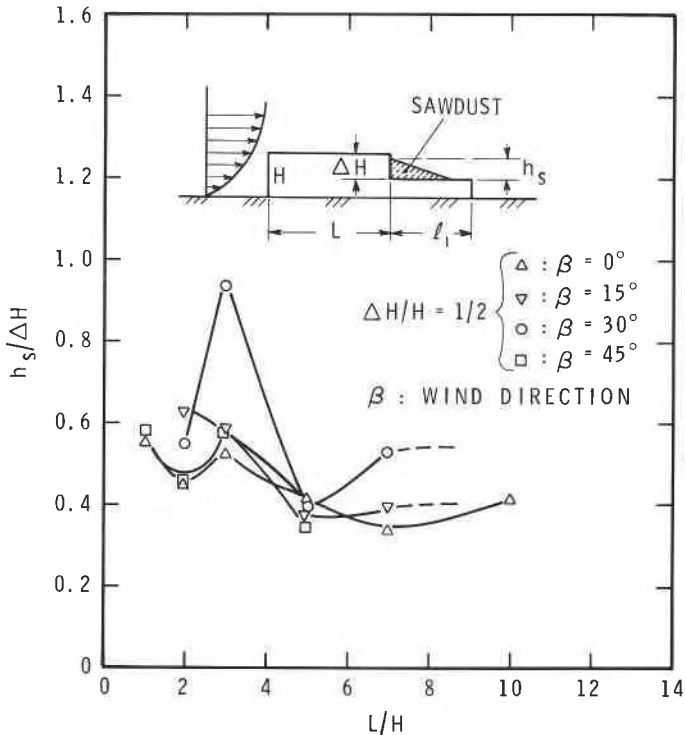


Fig. 7. Drift height as a function of wind direction β and aspect ratio of the upper roof, when $\Delta H/H=0.5$.

Figure 7 shows that the drift height varied with wind direction and aspect ratio of the main building. The maximum height ($h_s = 0.94 \Delta H$) was observed at $L/H=3$ with $\beta=30^\circ$. A change in the wind direction strongly affected the drift shape in the near-wake of the model in which $L/H=3$ (Fig. 7). However, the effect of wind direction was less spectacular for other models. From Fig. 7 it appears that h_s was not a function of the angle of incidence when $L/H=5$ and $\beta \geq 15^\circ$. This may indicate that the nature of flow in the recirculation region is stationary at angles of incidence between 15° and 45° . When $L/H=5$, the length of roof beyond the reattachment point is sufficient to start the redevelopment of a new boundary layer. For values of $L/H \geq 5$, the new boundary layer grows thicker with distance downstream. At the "step" the greater thickness allows a greater depth of snow to accumulate. This depends to some extent on β .

For buildings with $L/H \geq 5$, Fig. 7 shows that the sawdust accumulation has not reached the height of the upper roof - its maximum depth was only $0.54 \Delta H$. As noted previously, the width of the wind tunnel did not allow the use of models longer than $L/H=7$ at angles of attack β greater than 30° .

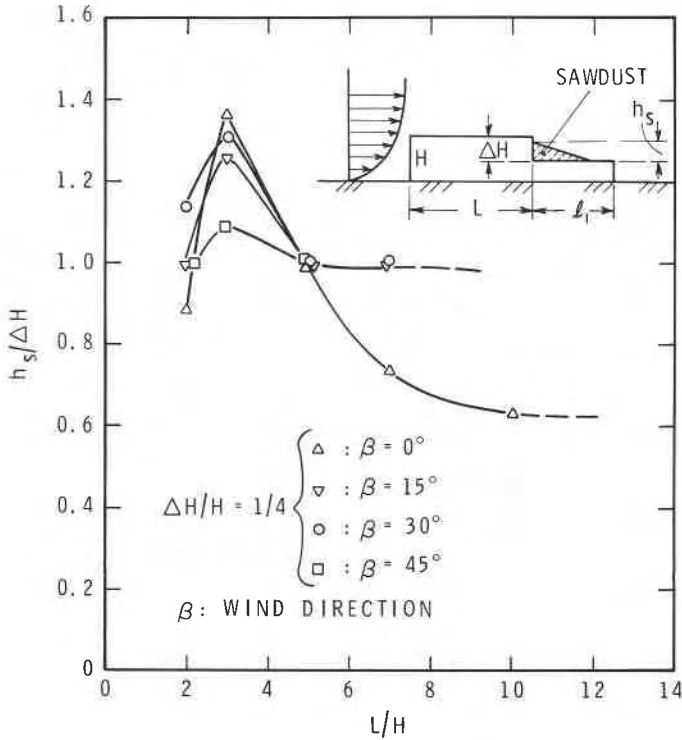


Fig. 8. Drift height as a function of wind direction β and aspect ratio of the upper roof, when $\Delta H/H=0.25$.

Case II: $\Delta H/H=1/4$.

Figure 8 shows that for long roofs ($L/H \geq 5$) with low values of ΔH there was no difference between the drift profiles obtained for all wind directions except $\beta=0^\circ$. With a decrease in $\Delta H/2$ to $H/4$, the vortex formation moved vertically upwards and the space between the upper and lower roofs was more rapidly filled with particles. The critical L/H ratio was 3 and the maximum h_s was observed at $\beta=0^\circ$. In water tunnel tests, the size of this vortex formation appeared to be greater than ΔH and could therefore result in h_s being higher than ΔH as shown in Fig. 8.

3.4.2. Estimate of the drift length l_s

The reattachment length of the lower roof, which is the horizontal distance between the trailing edge of the upper roof and the point of reattachment on the lower roof, can be obtained by analysis of shear stress profiles [15].

The maximum length of a drift on the lower roof is probably directly related to the reattachment length, as snow deposited downstream of the reattachment point would be carried away by the increasing speed of the shear layer.

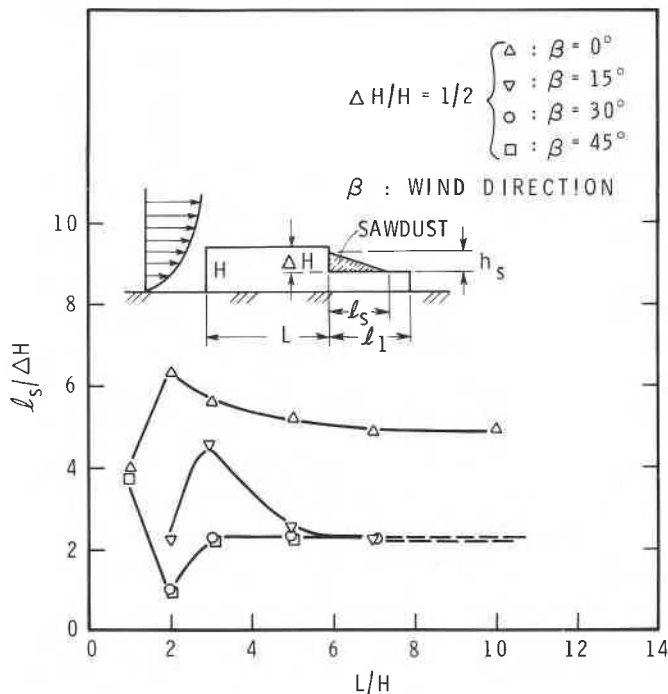


Fig. 9. Length of drift on lower roof as a function of wind direction β and aspect ratio of the upper roof when $\Delta H/H=0.5$

Case I: $\Delta H/H=1/2$.

The length of drift on the lower roof is plotted in Fig. 9 against the aspect ratio L/H of the upper building. At $\beta=0^\circ$ and $L/H=2$, l_s is $6.4 \Delta H$ but changes quite rapidly as the angle of incidence changes. As the aspect ratio L/H of the upper building is increased, l_s tends to reach a constant value of about $5 \Delta H$ when $\beta=0^\circ$, but drops to approximately $2 \Delta H$ as shown in Fig. 9 for values of β equal to 15° , 30° and 45° . Also the flow behaviour behind the upper building is only weakly affected by an increase in the angle of incidence for values of $L/H \geq 5$. For most design situations the National Building Code of Canada recommends that l_s be $2 \Delta H$, which is in good agreement only with tunnel results for $\beta \geq 15^\circ$ and $L/H \geq 5$. O'Rourke et al. [16] found from field data for many types of buildings and many $\Delta H/H$ ratios that $l_s/\Delta H$ was often greater than $2 \Delta H$. Their paper does not give enough information to allow actual drift lengths to be determined. Taylor's [14] data indicated, however, that $2 \Delta H$ was adequate for long buildings with $\Delta H/H$ of about 0.5 and lower roofs less than $5 \Delta H$ in length.

Case II: $\Delta H/H=1/4$.

For $L/H \geq 5$ a change in β from 15° to 45° resulted in an increase of l_s from

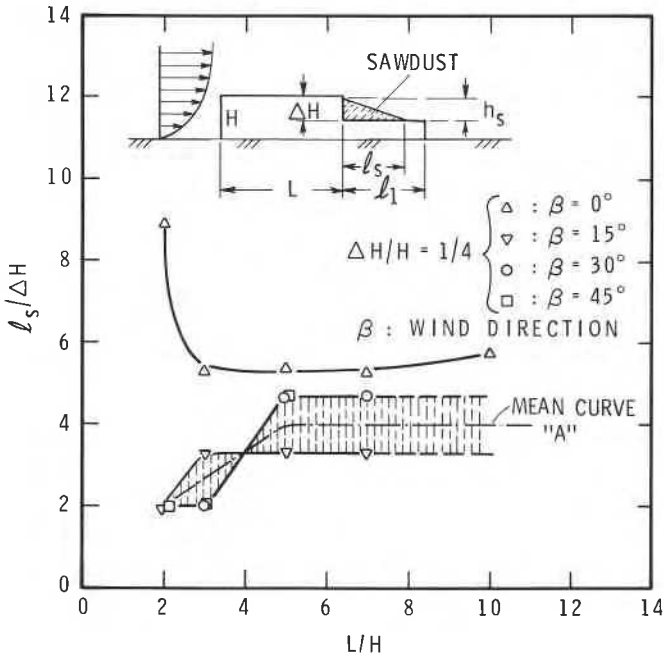


Fig. 10. Length of drift on lower roof as a function of wind direction β and aspect ratio of the upper roof when $\Delta H/H=0.25$.

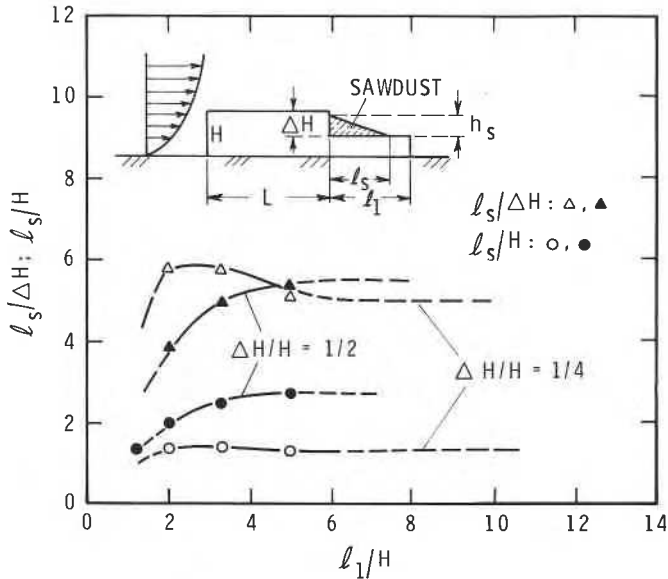


Fig. 11. Effects of lower roof length l_1 on length of drift on lower roof l_s when $L/H=10.0$, $\beta=0^\circ$.

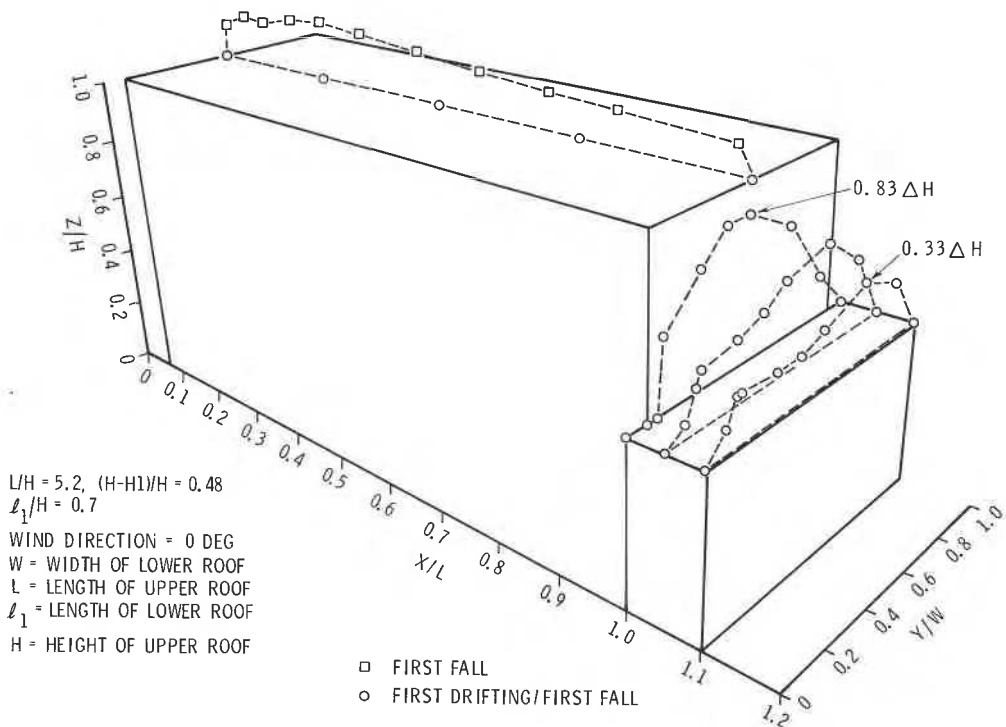


Fig. 12. Drift shape on a long model ($L/H=10$) with a short lower roof $l_1/H=0.7$.

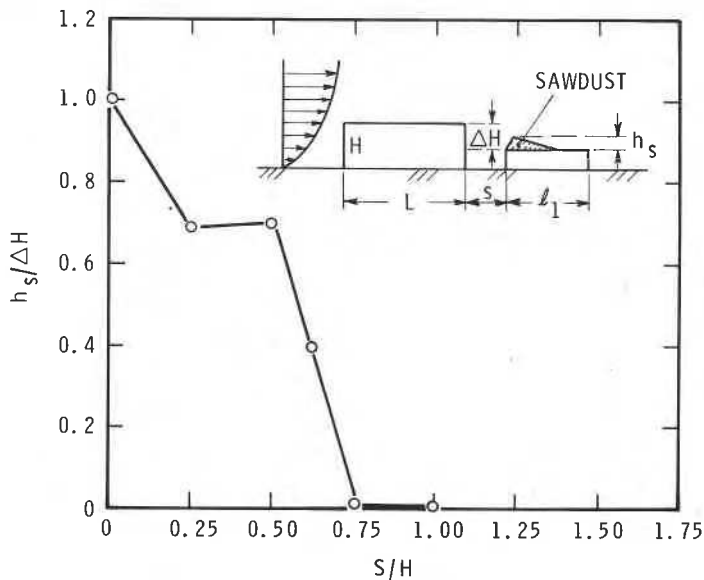


Fig. 13. Effect on drift height h_s of a gap between the upper and lower buildings. The effect is the same for $\Delta H/H=0.25$ and 0.50 .

$3.3\Delta H$ to $4.7\Delta H$ (Fig. 10). For short models, $L/H=3$, with $\beta=30^\circ$ and $L/H \geq 5$, the drift length tends asymptotically to $4.7 \Delta H$. In terms of loads this could be a significant difference from the results obtained when $\Delta H/H=0.5$ (Fig. 9).

The drift lengths obtained during the testing were in good agreement with most of the observations summarized by Eaton and Johnston [15] for conditions when β was 0° and when the free-stream turbulence was less than 1%.

Figures 9 and 10 reveal that, for models with $L/H \geq 3$ and $\beta=30^\circ$ and 45° , the nature of the recirculation in the near-wake is independent of the aspect ratio L/H . When $L/H \leq 3$, the free stream turbulence will cause an earlier reattachment of the flow and will move the centre of the reattachment bubble upstream towards the leading edge [17].

3.4.3. Effect of lower roof length on the length of drift for a long model ($L/H=10$)

The length of the lower roof is l_1 . Figure 11 shows that for l_1/H between 2 and 5, the drift length l_s decreases with an increase in $\Delta H/H$. For a long lower roof ($l_1/H \geq 5$), the drift length is independent of l_1 as shown in Fig. 11, probably because the maximum shear stress within the shear layer decreases rapidly downstream of the reattachment point [18]. For a short lower roof on the other hand ($l_1/H=0.7$) as shown in Fig. 12, the contact between the trailing edge of the lower roof and the shear layer from the trailing edge of the upper roof forces the vortices to form very close to the back face of the upper building.

The depth profile on the lower roof in Fig. 12 when $\beta=0^\circ$ is strong evidence of the large change in turbulence structure which occurs when the shear layer encounters the trailing edge of a short lower roof.

3.4.4. Effect of a gap between high and low buildings

When a gap S is introduced between a windward and leeward building, the height of the drift on the lower roof is reduced (Fig. 13). Figure 13 also shows that the non-dimensional gap width S/H strongly affects the drift height h_s on the lower roof. The kinetic energy of flow in the passage is increased due to the additional energy from flow along the sides of the building and the strength of the vortex system in the near-wake is reduced.

This results in an increased flow velocity near the lower roof and consequently a reduction in the deposition of particles there.

For gaps ranging from $0.25H$ to $0.50H$ (Fig. 13), the height of drifts is independent of the gap width. This suggests that the structure of the flow in the passage is stable and remains the same for this range of gap widths. The occurrence of a stationary vortex is probably the dominant phenomenon [19].

For $S/H \geq 5$, an increase in the gap width was accompanied by a large decrease in the drift size. Indeed, no drift was formed on the lower roof when S/H was greater than 0.75.

3.4.5. *Effects of wind velocities and snowfall on drift formation*

Figure 14(a) presents profiles of sawdust accumulation on a model building with $L/H=7.0$ and $\beta=30^\circ$. The aspect ratio of the lower roof was $l_1/H=3.25$. The effects of strong perturbations in the flow resulted in the leeward half of the upper roof being almost bare. As a result the maximum drift height $h_{s \max}$ is about $0.5\Delta H$ in the near-wake of the upper building.

The effect of more than one snowstorm is shown in Fig. 14(b). After the "second fall" the drift behind the upper building had a maximum height of about $0.5\Delta H$. With increased wind speed, this height increased to ΔH . The profile of the sawdust accumulation on the upper roof indicates that when $\beta=30^\circ$, the flow is split into two vortex streets which scour away the snow.

The next section compares experimental results with full-scale measurements on two buildings in Ottawa, Canada.

4. Comparison with field data

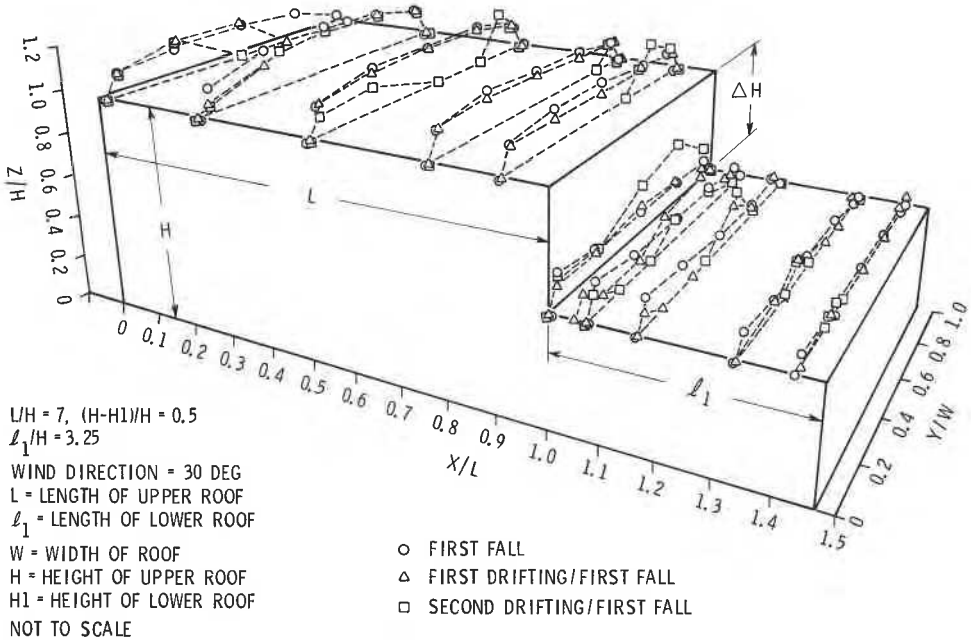
4.1. *Introduction*

The two buildings modelled, PWC and Ottawa Sufferance, are shown in Fig. 15 with their correct orientations and dimensions [14]. A heavy drift on Ottawa Sufferance is illustrated in Fig. 16. The roofs are in an industrial area of similar buildings of about the same height. The space between buildings is generally 45 m or more on each long side although there is a large warehouse parallel to the long side of the PWC building and 15 m away on the north side. To the south-west of the PWC building there are houses 400 m away while buildings to the ENE of Ottawa Sufferance are more than 500 m distant. The terrain is flat with the occasional tree no higher than the buildings. This is unusually open terrain upstream which satisfies the conditions in eqn. (3) and Section 3.2.1.

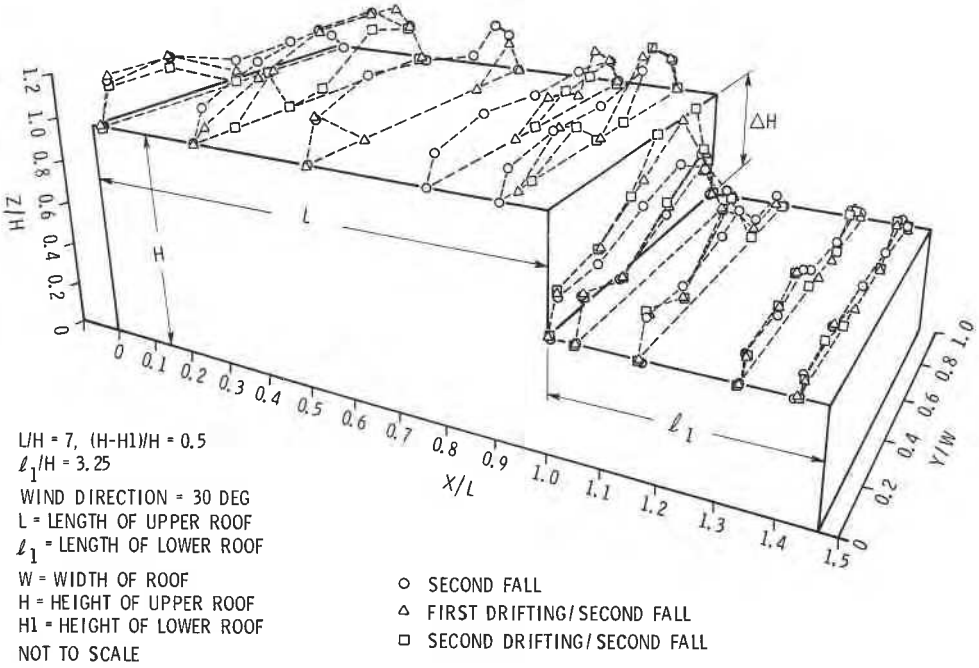
Figure 17 illustrates the variation of the maximum drift load from year to year and shows that during short surveys major peaks could be missed entirely. For example, for a period of four years from 1974 to 1977 the maximum drift load on Ottawa Sufferance was less than 55% of the maximum measured during a period of 10 years. Thus field surveys should be conducted over long periods (usually at least ten years). As such surveys are expensive, it is clear that an effective modelling technique would save a lot of time and money if it reduced the need for such surveys.

4.2. *Comparison of drifts on full-size and model buildings*

Because the models were too long to be rotated fully in the tunnel, it was important to search the meteorological records for snowstorms with winds blowing in the same direction as those modelled in the wind tunnel. Further snowstorms that occurred early in Ottawa winters and deposited large drifts



(a)



(b)

Fig. 14. Effect of wind velocity and snowfall on drift formation: (a) first fall, (b) second fall.

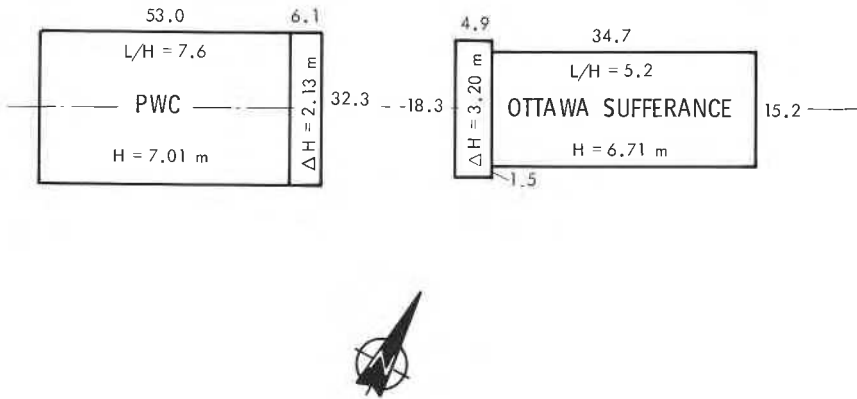


Fig. 15. Plan view of buildings showing sizes and orientations to true north. It should be noted that the scales are different from building to building. ΔH is the difference in elevation between the upper and lower flat roofs.

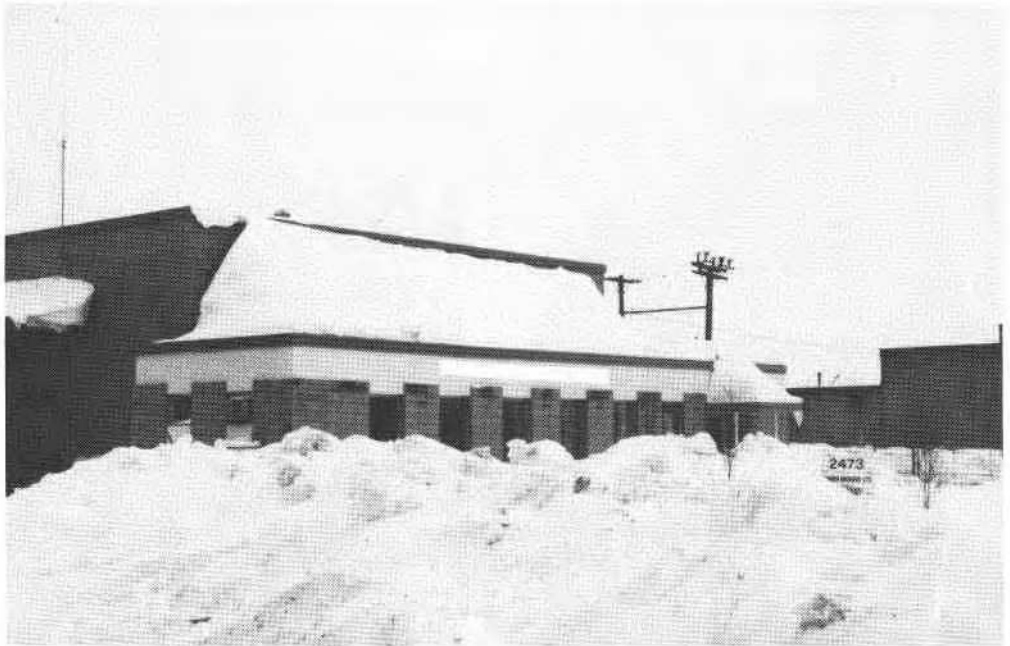


Fig. 16. Large "triangular" drift in the lee of the upper roof of Ottawa Sufferance, mid-January 1978 ($\Delta H/H = 0.48$).

on roofs completely bare prior to the storms would have been ideal. This seldom occurred.

Ottawa Sufferance Warehouse ($L/H = 5.2$, $\Delta H/H = 0.48$).

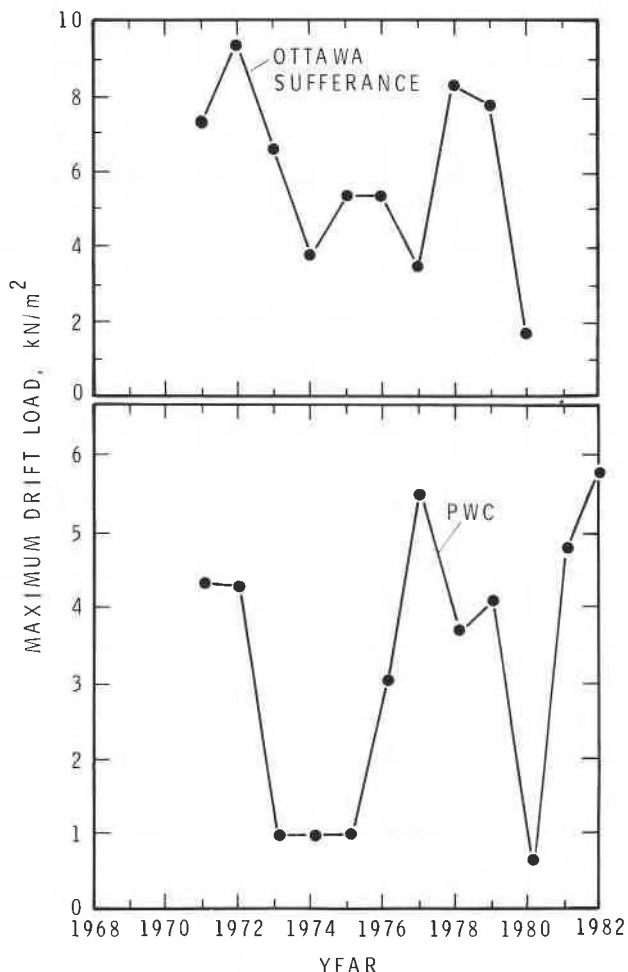


Fig. 17. Variation of the annual maximum drift load on two two-level flat roofs in Ottawa.

The model of this building was tested at an angle of attack $\beta=0^\circ$. On the full-size building this corresponded to winds from the ENE. On four occasions large drifts were deposited but the conditions did not correspond to the ideal situation. Indeed the measurements (Fig. 18) and photograph taken on 23 January 1978 (Fig. 16) followed a succession of snowfalls almost daily from mid-November with winds from all directions, although a good number were from the ENE. In December 1977 there were four major snowfalls: 18.0 cm on the 6th with average ENE winds at 27.6 km h^{-1} ; 21.6 cm on the 9th with east winds at 28.2 km h^{-1} ; 12.8 cm on the 14th with ENE winds at 16.1 km h^{-1} ; 30.4 cm on the 21st with ENE winds averaging 21.3 km h^{-1} . Temperatures were below zero throughout this period. The last two events were on 8 January when 10.0

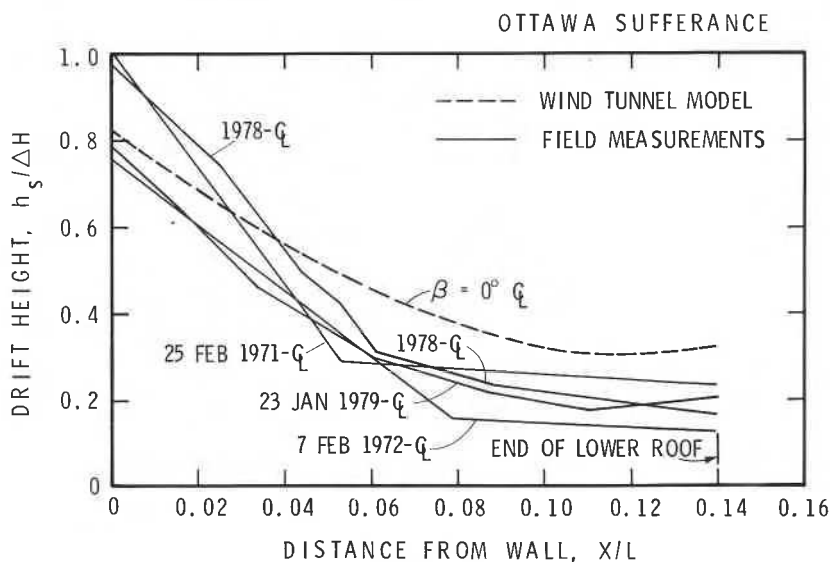


Fig. 18. Non-dimensional profiles of heights and lengths of drifts measured on the centre-line C_L of the lower roof.

cm fell at temperatures between $+2.0$ and -11.0°C with average winds of 14.1 km h^{-1} East, and on 18 January when 10.2 cm fell at temperatures between -5.7 and -15.4°C with average winds of 19.8 km h^{-1} NNE.

The other three profiles in Fig. 18 were observed: (1) after a snowstorm of 30 cm on 23 February 1971 (highest temperature -3.9°C) with the readings taken on the 25th (temperature between -10°C and 0°C); (2) following a snowstorm on 3 and 4 February 1972 (highest temperature -3.3°C) with readings on 7 February (temperature between -3.3 and -23.3°C overall); (3) after a snowstorm on 21 January 1979 (highest temperature -4.4°C) with readings taken on the 23rd (temperature between -4.4 and -14.4°C overall).

The dashed line in Fig. 18, presenting the model results, is similar to the profiles of depths measured along the building centre-line during the four storms, although the depth would increase or decrease depending on the combinations of snowfall and winds used during testing. It is important to note that these depth measurements were occasionally exceeded by profiles at other locations after storms in which $\beta \neq 0^\circ$.

The PWC building ($L/H=7.6$, $\Delta H/H=0.30$).

The direction of winds blowing down the centreline of this building is WSW. As the model was small enough to rotate 15° in the tunnel, the influence of a 15° shift in wind direction could be studied. It is clear from the dashed lines in Fig. 19 that varying β from 0° to 15° makes a significant difference in the depth

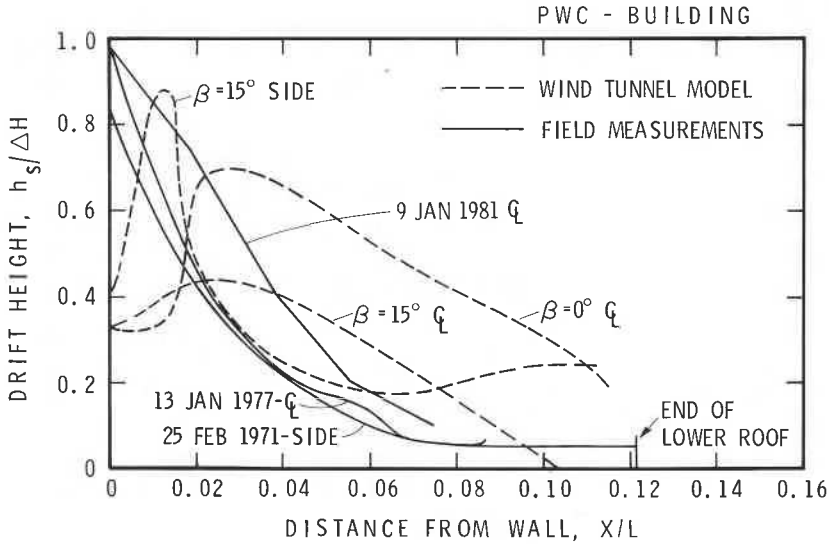


Fig. 19. Non-dimensional profiles of the heights and lengths of drifts measured on the centre-line C_L and at the side of the lower roof.

profiles at the centreline of the model. At the full-size building the natural wind would not cooperate. β varied enormously during storms. As there was a large flat-roofed building about 5 m higher and 15 m to the north and parallel to the PWC building, winds blowing from the north-west passed over some portion of it before arriving over the PWC building. The buildings were too large for both to be modelled together in the tunnel.

The snowfall in the winter of 1970–1971 was very heavy with 111 cm falling in December, 76.5 cm in January and 157.5 cm in February up to the 25th. On 13 February 1971, 32 cm of snow fell accompanied by winds averaging 26 km h^{-1} from the NNW. On the 14th, winds at 22–40 km h^{-1} blew from the west for 13 h and on the 15th at 5–18 km h^{-1} from the west, south-west and WSW for 11 h. The resulting snow load profile at the side of the roof compares favourably with that for $\beta=15^\circ$ at the side of the model except near the wall where strong axial vortices are likely to affect the drifting.

A profile of snow depths recorded at the centre-line of the roof on 13 January 1977 is also plotted in Fig. 19. On 10 January, 23.2 cm of snow fell accompanied by strong wind averaging 27.8 km h^{-1} (ENE) and gusting to 46.3 km h^{-1} (ENE). This wind blew in a direction 180° from that expected to give the maximum drift on the roof. During 11 and 12 January, however, another 2.4 cm fell with winds from the west averaging 11–20 km h^{-1} . Although the resulting snowdrift was deep at the wall, it dropped away very steeply, its slope more resembling the model prediction for $\beta=15^\circ$ than for $\beta=0^\circ$.

In 1981, results were recorded on 9 January, three days after a fall of 12.6

cm of snow. Although the wind was mostly from the south while the snow fell, on the 7th and 8th the wind was largely from the west ($\beta=22.5^\circ$) averaging about 19 km h^{-1} , and on the 9th it came from the east and south at only 8.5 km h^{-1} . The depth profile recorded at the centre-line of the roof is also shown in Fig. 19. The snow depths exceed those recorded on the model by a large amount near the wall but farther away, snow depths are considerably less than those indicated by the model.

It is apparent that although some of the drifts measured on the PWC building resemble in shape some of those obtained in the tunnel, the time variability of wind direction resulting in high drifts was too complex to be modelled in the tunnel used.

5. Summary and conclusions

Modelling criteria were developed to select a suitable particle to simulate the heights and lengths of snow drifts on roofs. Visualization of the flow process in a water tunnel led to the observation that the vortex system on the roof surface throws up the modelling particles in clouds. Comparison of wind tunnel measurements with field observations leads to the following conclusions.

1. Turbulent transport of snow along an upper roof is the main mechanism for drift formation in its near-wake. Such transport is strongly affected by changes in the after-body length. Results from the wind indicate that the maximum drift occurs when the length of the upper roof is about three times its height.

2. The wind tunnel testing also indicates that the height and length of drifts depend primarily on the behaviour of the separated flow over the upper roof. The maximum height could be as much as 40% greater than the difference in elevation, ΔH between the upper and lower roofs when this difference is relatively low ($\Delta H/H \approx 0.25$) and when the angle of attack β is constant at 0° .

3. The introduction of a gap between a windward and leeward building results in a reduction in the deposition of particles on the lower roof due to increased flow velocity near the lower roof. Model tests indicate that for a gap greater than 75% of the upper roof height, no drift forms on the lower roof. There are no field data to confirm this.

4. There are similarities between the geometry of snowdrifts on roofs modelled in the wind tunnel and those on full-size buildings. Some of the differences in drift height and shape were due to the time variations in wind direction outdoors, variations that could not be simulated in the tunnel.

5. Some discrepancies between model and full scale arise because a wind tunnel can only model aerodynamic effects and also because the upstream geometry was not modelled exactly in the wind tunnel. It cannot account for the influence of heat loss, solar radiation, changes in humidity, air temperatures and rainfall. These all affect snow density, scouring and drifting.

Acknowledgements

The authors are grateful for advice and support from W.A. Dalglish and for the assistance of J.D. Atkins and Yves Grenier with the wind tunnel testing and P.J. Daly with the field measurements of snow depths and densities. They would also like to acknowledge the use of the wind tunnel facility at the hydraulics laboratory of the Division of Mechanical Engineering, NRC, and the willing cooperation of Dr. Bruce Pratte. They are grateful for the advice of R.L. Wardlaw and for the loan of equipment from the Low Speed Aerodynamics Section of the National Aeronautical Establishment, NRC.

This paper is a contribution from the Institute for Research in Construction, National Research Council of Canada. Copyright in the paper belongs to the Crown in right of Canada, i.e. to the Government of Canada.

References

- 1 G.H. Strom, G.R. Kelly, E.L. Keitz and R.F. Weiss, Scale model studies on snow drifting, Res. Report No. 73 (U.S. Army, Snow, Ice and Permafrost Research Establishment, Hanover, NH), September 1962, 50 pages.
- 2 R.A. Bagnold, *The Physics of Blown Sand and Desert Dunes*, Methuen, London, 1954, 265 pages.
- 3 E.A. Finney, Snow drift control by highway design; results of wind tunnel investigations interpreted, *Roads Streets*, 83 (3) (1940) 45-48.
- 4 J.D. Iversen, Drifting snow similitude: drift deposit rate correlation, Proc. 5th Int. Conf. on Wind Engineering, July 8-14 1979, Fort Collins, CO, pp. 1035-1047.
- 5 D. Kobayashi, Studies on snow transport in low-level drifting snow, Institute of Low Temperature Science, Hokkaido University, Japan, Series A, No. 24, 1972, pp. 1-58.
- 6 N. Isyumov, An approach to the prediction of snow loads, Ph.D. Thesis, University of Western Ontario, London, Ont., Research Report BLWT-9-71, 1971, 534 pages.
- 7 J.S. de Krasinski and W. Anson, The study of snow drifts around the Canada Building in Calgary, Report No. 71, October 1975, University of Calgary, Dept. Mechanical Engineering.
- 8 J.S. de Krasinski and T. Szuster, Some fundamental aspects of laboratory simulation of snow or sand drifts near obstacles, Report No. 151, 1979 (University of Calgary, Dept. Mechanical Engineering).
- 9 T. Szuster and J.S. de Krasinski, Experimental methods and techniques related to laboratory study of snow drift formation near obstacles on the ground, Report No. 154, 1980 (University of Calgary, Dept. Mechanical Engineering).
- 10 A.K. Dyunim, Vertical Distribution of Solid Flux in a Snow-Wind Flow. Technical Translation 999, National Research Council of Canada, 1961, 16 pages (translated into English by G. Belkov).
- 11 M. Jensen and N. Franck, *Model-Scale Tests in Turbulent Wind, Part I*, The Danish Technical Press, Copenhagen, 1963, 96 pages.
- 12 R.J. Kind, A Critical Examination of the Requirements for Model Simulation of Wind-Induced Ground-Drift or Erosion Phenomena in Wind Tunnels with Particular Emphasis on Snow Drifting, LTR-LA-167, August 1974 (National Research Council of Canada, National Aeronautical Establishment).
- 13 N.J. Cook, Wind tunnel simulation of the adiabatic atmospheric boundary layer by roughness, barrier and mixing-device methods, *J. Ind. Aerodyn.*, 3 (1978) 157-176.

- 14 D.A. Taylor, Snow loads on two-level flat roofs, Proc. Eastern Snow Conf. V29, 41st Annu. Meet., Washington, DC June 7-8, 1984, pp. 3-13. Also National Research Council of Canada, Division of Building Research, reprint No. NRCC 24905, Ottawa.
- 15 J.K. Eaton and J.P. Johnston, A review of research on subsonic turbulent flow reattachment, AIAA J. 19(9) (1981) 1093-1100.
- 16 M.J. O'Rourke, R.S. Speck and U. Stiefel, Drift snow loads on multilevel roofs, Proc. Eastern Snow Conf. V29, 41st Annu. Meet., Washington, DC, June 7-8 1984, pp. 14-25. Also ASCE J. Constr. Div., 111, (2) (1985) 290-306.
- 17 F. da Matha Sant'Anna, Contribution à la compréhension de l'écoulement autour des corps prismatiques à section rectangulaire. Thèse de doctorat (Ph.D.), Université de Sherbrooke, Quebec, January 1983.
- 18 P. Bradshaw and F.Y.F. Wong, The reattachment and relaxation of a turbulent shear layer, J. Fluid Mech., 52 (1) (1972) 113-135.
- 19 A. Diemling, I. Kronke, F. Schramke and H. Sockel, Wind-induced vibrations of a facade element, J. Wind Eng. Ind. Aerodyn., 11 (1983) 133-148.

Appendix A: Derivation of equations 9 and 10

The governing equations of motion for a particle are:

$$\ddot{x}_m + \frac{K_{0m}}{M_m} \dot{x}_m = \frac{K_{0m}}{M_m} K_{1m} y_m \quad (\text{A1})$$

$$\ddot{y}_m + \frac{K_{0m}}{M_m} \dot{y}_m + g = 0 \quad (\text{A2})$$

where subscript m represents the model scale. Equations (A1) and (A2) are identical with eqns. 7 and 8.

For similarity conditions, eqn. 5 gives:

$$y_m = \bar{l}y \quad \dot{y}_m = \bar{U}\dot{y} \quad \dot{x}_m = \bar{U}\dot{x} \quad (\text{A3})$$

$$M_m = \bar{\rho}\bar{d}^3 M \quad K_{0m} = \bar{d} K_0 \quad K_{1m} = K K_1 \quad (\text{A4})$$

In addition, acceleration of the particle in non-dimensional terms can be derived as follows

$$\ddot{i}_m = \frac{d\dot{i}_m}{dt} = \frac{\partial \dot{i}_m}{\partial l_m} \frac{\partial l_m}{\partial t} = \dot{i}_m \left(\frac{\partial \dot{i}_m}{\partial l_m} \right) \quad (\text{A5})$$

from eqn. 5:

$$\dot{i}_m = \bar{U}\dot{i} \quad (\text{A6})$$

$$\ddot{i}_m = \bar{U}\dot{i} \left(\frac{\partial \dot{i}_m}{\partial l_m} \right) \quad (\text{A7})$$

The term in brackets is also expressed as a function of non-dimensional parameters

$$\frac{\partial \dot{l}_m}{\partial l_m} = \frac{\partial \dot{l}_m}{\partial \bar{l}} \frac{\partial \dot{l}}{\partial l} \frac{\partial l}{\partial l_m} \quad (\text{A8})$$

The right terms are products of three quantities and eqn. 5 gives

$$\frac{\partial l}{\partial l_m} = \frac{1}{\bar{l}} \quad \text{and} \quad \frac{\partial \dot{l}_m}{\partial \bar{l}} = \bar{U}$$

Then

$$\frac{\partial \dot{l}_m}{\partial l_m} = \bar{U} \frac{1}{\bar{l}} \frac{\partial \dot{l}}{\partial l} \quad (\text{A9})$$

From eqn. (A5),

$$\ddot{l}_m = \bar{U} \dot{l} \bar{U} \frac{1}{\bar{l}} \frac{\partial \dot{l}}{\partial l} \quad (\text{A10})$$

or

$$\ddot{l}_m = \frac{\bar{U}^2}{\bar{l}} \left(\dot{l} \frac{\partial \dot{l}}{\partial l} \right) \quad (\text{A11})$$

The term $\dot{l} \partial \dot{l} / \partial l$ has the same units as \ddot{l}_m and it is assumed that this term is equivalent to \ddot{l} . Thus

$$\ddot{l}_m = \frac{\bar{U}^2}{\bar{l}} \ddot{l} \quad (\text{A12})$$

Similarly,

$$\ddot{x}_m = \frac{\bar{U}^2}{\bar{l}} \ddot{x} \quad \ddot{y}_m = \frac{\bar{U}^2}{\bar{l}} \ddot{y} \quad (\text{A13})$$

The various non-dimensional parameters are introduced in eqns. (A1) and (A2) to obtain:

$$\frac{\bar{U}^2}{\bar{l}} \ddot{x} + \frac{K_0}{M} \frac{\bar{U}}{\bar{\rho} \bar{d}^2} \dot{x} = \frac{K_0}{M} \frac{K \bar{l}}{\bar{\rho} \bar{d}^2} K_1 \quad (\text{A14})$$

$$\frac{\bar{U}^2}{\bar{l}} \ddot{y} + \frac{K_0}{M} \frac{\bar{U}}{\bar{\rho} \bar{d}^2} \dot{y} + g = 0 \quad (\text{A15})$$

Appendix B: Derivation of time scaling

Governing equations use Newton's second law:

$$\Sigma F_{\text{ext}} = Ma \quad (\text{B1})$$

or

$$Ma = F + Mg \quad (B2)$$

Equation (B2) in terms of x and y is:

$$-M \frac{d\dot{x}}{dt} = D_x \quad \text{and} \quad -M \frac{d\dot{y}}{dt} = D_y + Mg \quad (B3)$$

where D_x and D_y are, respectively, drag along the x and y directions. The vertical velocity component of the fluid is zero (i.e. $D_y = 0$), thus

$$\frac{d\dot{y}}{dt} = 0 \quad (B4)$$

Now

$$M = \rho \frac{4}{3} \pi r^3 \quad r = \frac{d}{2}$$

and drag

$$D_x = \frac{1}{2} C_{D_x} \pi r^2 \rho_f \dot{x}^2$$

where ρ is the particle density, d is the particle characteristic diameter, ρ_f is the fluid density, and C_{D_x} represents the drag coefficient along the x direction.

The governing equation of particle movement is:

$$-M \frac{d\dot{x}}{dt} = D_x \quad (B5)$$

Then

$$-\frac{4}{3} \rho \pi \frac{d^3}{8} \frac{d\dot{x}}{dt} = \frac{1}{2} C_{D_x} \pi \frac{d^2}{4} \rho_f \dot{x}^2$$

or

$$\frac{4}{3} \rho d \frac{d\dot{x}}{dt} + C_{D_x} \rho_f \dot{x}^2 = 0 \quad (B6)$$

Equation (B6) is a simple form of the general form of particle movement in air. Similarly for a model particle,

$$\frac{4}{3} \rho_m d_m \frac{d\dot{x}_m}{dt_m} + (C_{D_x})_m \rho_{fm} \dot{x}_m^2 = 0 \quad (B7)$$

Various non-dimensional parameters have been defined in Appendix A:

$$\rho_m = \bar{\rho} \rho \quad d_m = \bar{d} d \quad \dot{x}_m = \bar{U} \dot{x} \quad (B8)$$

and similarly:

$$\rho_{fm} = \bar{\rho}_f \rho_f \quad t_m = \bar{t} t \quad (C_{D_x})_m = \bar{C}_{D_x} C_{D_x} \quad (\text{B9})$$

From eqn. (B7):

$$\frac{4}{3} \rho d \left(\frac{\bar{U}}{\bar{\rho} \bar{t}} \right) \frac{d\dot{x}}{dt} + C_{D_x} (\bar{C}_{D_x} \bar{\rho}_f \bar{U}^2) \rho_f \dot{x}^2 = 0 \quad (\text{B10})$$

From comparison of eqns. (B6) and (B10) one can write:

$$\frac{\bar{U}}{\bar{\rho} \bar{t}} \bar{d} = 1 \quad (\text{B11})$$

$$\bar{C}_{D_x} \bar{\rho}_f \bar{U}^2 = 1 \quad (\text{B12})$$

Time scaling will be given by eqn. (B11). Then,

$$\frac{\rho_m}{\rho} \frac{d_m}{d} \frac{\dot{x}_m}{\dot{x}} = \frac{t_m}{t} \quad (\text{B13})$$

If ρ , d , \dot{x} and t are associated with the prototype particle (in full-scale), then:

$$\frac{t_m}{t_p} = \frac{\rho_m}{\rho_p} \frac{d_m}{d_p} \left(\frac{l_m}{l_p} \right)^{1/2} \quad (\text{B14})$$

with

$$\frac{\dot{x}_m}{\dot{x}_p} = \left(\frac{l_m}{l_p} \right)^{1/2} \quad (\text{see eqn. (15)})$$

In terms of z_{0m} and z_{0p} (roughness length)

$$\frac{t_m}{t_p} = \frac{\rho_m}{\rho_p} \frac{d_m}{d_p} \left(\frac{z_{0m}}{z_{0p}} \right)^{1/2} \quad (\text{B15})$$

This equation is identical with eqn. 22.

This paper is being distributed in reprint form by the Institute for Research in Construction. A list of building practice and research publications available from the Institute may be obtained by writing to Publications Section, Institute for Research in Construction, National Research Council of Canada, Ottawa, Ontario, K1A 0R6.

Ce document est distribué sous forme de tiré-à-part par l'Institut de recherche en construction. On peut obtenir une liste des publications de l'Institut portant sur les techniques ou les recherches en matière de bâtiment en écrivant à la Section des publications, Institut de recherche en construction, Conseil national de recherches du Canada, Ottawa (Ontario), K1A 0R6.